PEROVSKITE-BASED NANOMATERIALS FOR METAL-ION BATTERIES: A MINI-REVIEW.

Fayed, M. G. [*] ***and Mohamed, S. G.*** [*,†]

[*] *Mining and Metallurgy Engineering Department, Tabbin Institute for Metallurgical Studies, (TIMS), Tabbin, Helwan 109, Cairo 11421, Egypt.*
[†] *Corresponding Author Email: saadmohamed@tims.gov.eg*

ABSTRACT

The most promising possible candidate for significant scientific advancements in widely used renewable energy-storage devices, including supercapacitors, batteries, fuel cells, solid oxide fuel cells, and solar-cell applications, is perovskite-based electrode materials. Perovskite compounds have been utilized as electrode materials for metal-ion batteries and have demonstrated significant electrochemical properties. The rising demand for electric vehicles has intensified research efforts to improve metal-ion battery performance by increasing power density, energy density, and cycle stability. Perovskites' unique structural and physicochemical properties make them one of the most important compounds in various applications. Recently, perovskites and their composites have been classified as a novel category of pioneered materials for metal ion batteries. Compared to graphite and Li_4Ti5O_{12}, the perovskites have excellent cycling and charge storage capacity performance. This review covers the most recent developments in perovskites and their composites that are utilized as electrode materials in lithium and sodium-ion batteries and discusses the previous literature on oxide perovskites and organic-inorganic perovskites utilized as electrode materials for metal-ion batteries.

Keywords

Perovskites; Lithium-ion battery; Sodium-ion battery; Nanomaterials.

Abbreviations list

A g^{-1}	Ampere per gram
CNO	$Ce_{1/3}NbO_3$
C-rates	Current rate
CV	Cyclic Voltammetry
DMC	Dimethyl carbonate
D-ZSO	Double-shell $ZnSnO_3$
EC	Ethylene carbonate
GO	Graphene oxide
LIB	Lithium-ion battery
LLTO	$Li_{0.33}La_{0.56}TiO_3$

LNMO	$LiNi_{0.5}Mn_{1.5}O_4$
LTO	$Li_4Ti_5O_{12}$
mAh g^{-1}	Milliampere hour per gram
MIB	Metal-ion battery
NBTO	$Na_{0.5}Bi_{0.5}TiO_3$
NCM811	$LiNi_{0.8}Co_{0.1}Mn_{0.1}O_2$
SEI	Solid electrolyte interphase
SEM	Scanning electron microscope
SIB	Sodium-ion battery
STO	$SrTiO_3$
XRD	X-ray diffraction
Y-ZSO	Yolk-shell $ZnSnO_3$
ZSCs	Nanocubes $ZnSnO_3$
ZSO	$ZnSnO_3$
ZSSs	Nanosheets $ZnSnO_3$

1. METAL-ION BATTERY (MIB)

Russian and German mineralogists discovered the first Perovskite mineral in Russia, which was named by August Kämmerer. Perovskites are suitable for usage in a variety of applications according to their fascinating features, which have led to intense research on them in recent years. These applications include electronic conduction, superconductivity, magnetic resistance, dielectric properties, ferroelectricity, and piezoelectricity. It is commonly regarded that the general formula for perovskite compounds derives from ABO_3, which has the structure of a $CaTiO_3$ compound. It is noteworthy that perovskite materials may contain 90% of the metallic elements in positions A and/or B of the periodic table while preserving their distinctive perovskite structure. The typical formula for the cubic crystal structure of ideal perovskite oxides is ABO_3 [1].

By studying the chemical formulae, it was known that A stands for a rare or alkaline earth metal and B is a transition metal, such as $SrTiO_3$. According to figure 1, the Sr atom coordinates to 12 oxygen atoms residing in the A-site, whereas Ti is in the B-site coordinates to 6 atoms. Perovskites with various microstructures have been produced utilizing a variety of chemical techniques, which allows them to compete with the materials now utilized as electrodes in various kinds of batteries. Due to its versatile features, perovskite compounds are being used in industrial products like batteries, memory storage devices, photovoltaic solar cells, piezoelectric devices, capacitors, and fuel cells. There is a scientific and societal imperative to use renewable energy sources

since fossil fuel supplies are being depleted quickly, traditional energy sources emit large amounts of gas, the world is warming, and energy demand is rising. The lack of continuity is one of the main issues with the utilization of renewable energy sources. Hence, when employed under particular circumstances, energy storage systems must be used in combination with a variety of renewable energy sources. The development of new metal ion battery (MIB) materials may allow the use of MIBs in markets for grid-scale storage electric and plug-in hybrid vehicles. The most competitive candidate and superior to all other MIBs as energy storage technologies is the lithium-ion battery (LIB).

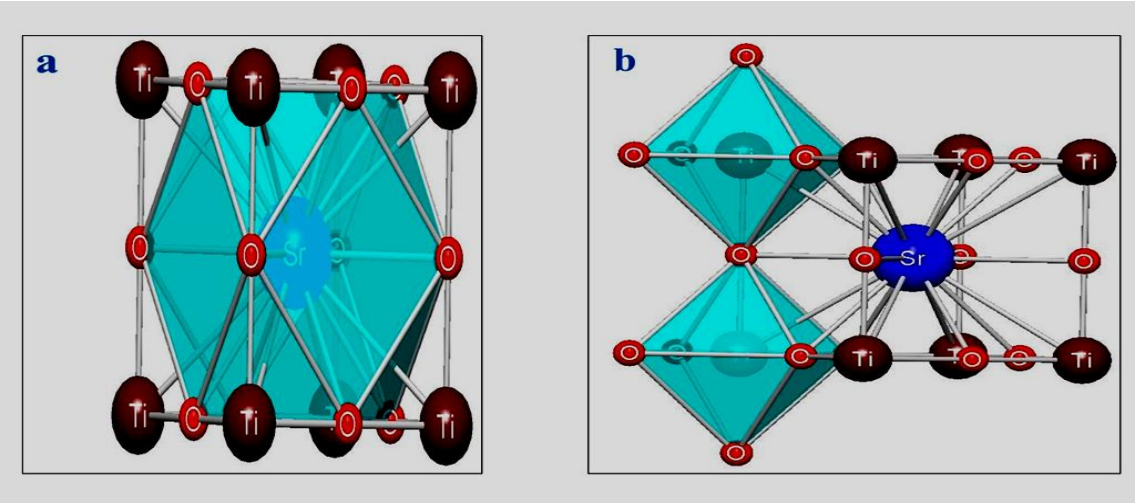

Fig. 1: Cubic crystal structure of perovskite $SrTiO_3$ a) Sr atom coordinates by 12 oxygen atoms, b) Ti atom coordinates by 6 oxygen atoms.

2. LITHIUM-ION BATTERY (LIB)

The manufacture and use of LIB have been amazing in the last two decades and changed our life's course. Additionally, it frequently has the largest market share in the electronics sector, which provides the portable power used by laptops, digital cameras, tablets, and mobile phones. It is a promising energy source for plug-in hybrid and electric vehicles. Meanwhile, graphite is a common intercalation/deintercalation compound applied as an anode material in commercial LIBs. It retains capacity well, is affordable, and has strong electronic conductivity. The LIBs are based on a unique electrochemical reaction, where the lithium-ion is transferred between negative and positive electrodes through the electrolyte phase on discharge and charge processes. The commonly utilized LIBs comprise graphite with a layered structure as a negative electrode (anode) coated on copper used as a current collector.

The positive electrode is a layer-type $LiCoO_2$ coated on aluminum used as a current collector. Polypropylene separator, used to prevent short circuit, is soaked in a nonaqueous electrolyte made of a high conductive salt $LiPF_6$ dissolved in a blend of alkyl carbonate organic solvents, as illustrated in figure 2 [2, 3]. However, owing to the low operating voltage (0.2 V), poor rate capability, theoretical capacity (372 mAh g^{-1}) is low, which does not satisfy the ambitions of the new generation batteries, low volumetric capacity (830 mAh mL^{-1}), and the growth of lithium dendrite observed in

the graphite anode can lead to serious safety concerns [4, 5]. It cannot keep up with the rising demand for next-generation LIBs. $Li_4Ti_5O_{12}$ (LTO) is thought to be a viable LIB-negative electrode material. [6]. Excellent safety reliability and exceptional cyclability result from LTO's high voltage of the reduction (1.5 V vs. Li/Li^+). Additionally, throughout the cycling process, LTO displays a minor volume change, a steady voltage plateau, and a high rate of Li-ion diffusion. Unfortunately, among all intercalation materials, LTO possesses low theoretical and volumetric capacities of 175 mAh g^{-1} and 612 mAh mL^{-1}, respectively. LTO is challenging to utilize as an appropriate negative electrode material for next generation LIBs. Hence, finding alternatives with good insertion potential is essential, high capacity, and safety potential, in contrast to LTO or graphite [7, 8].

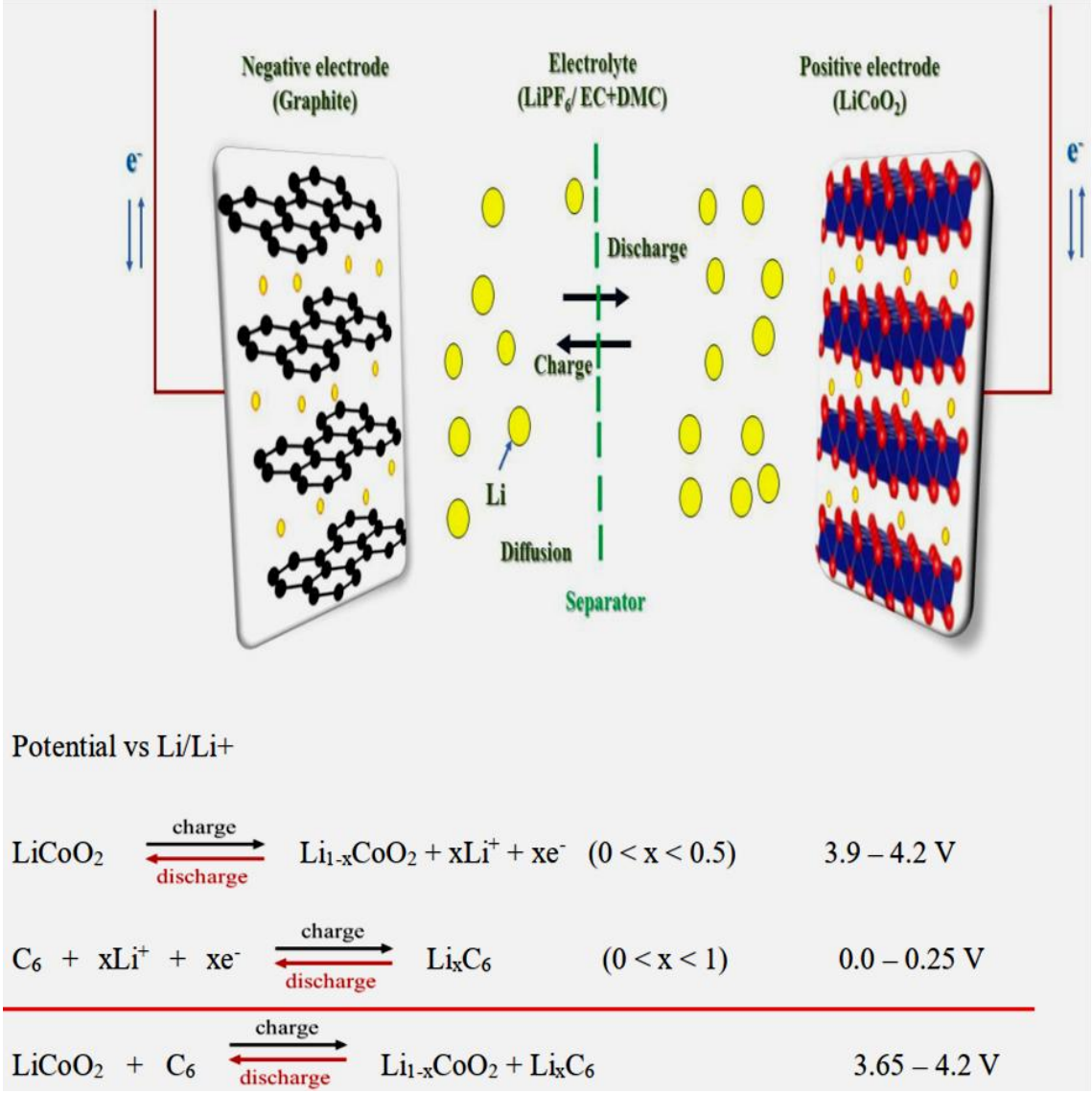

Fig. 2: The first commercialized Lithium-ion battery components, $LiCoO_2$, graphite, and $LiPF_6$ in EC+DMC and reactions path during charge and discharge processes.

Perovskites' unique crystal structure provides significant advantages over graphite and LTO because they can solve this issue. Numerous oxide perovskites have been utilized as anodes for LIBs and have demonstrated significant electrochemical performance. The most used and extensively studied compounds are bimetal oxides with chemical formula $MM`O_3$ (M=Zn, Ca, Ba, Co, Li) and (M`= Sn, Fe, Nb, Ni).

Theoretically, the $ZnSnO_3$ (ZSO) compound has a high capacity of (1317 mAh g^{-1}). The extra capacity originated from the reaction of zinc with Li through the alloying-dealloying process.

Hence, ZSO is the most promising perovskite compound and is expected to be utilized as an environmental-friendliness and cheap electrode material in metal ion batteries. ZSO powders have been prepared with various morphologies, where G. Ma *et al.* synthesized $ZnSnO_3$ nanorods by a facile template route.

P. Barquinha *et al*. used a hydrothermal method for preparing $ZnSnO_3$ nanowires [9]. $ZnSnO_3$ hollow fibers have been decorated utilizing biotemplate cotton by Z. Yang *et al*. [10]. Chen *et al.* synthesized $ZnSnO_3$ nanocubes (ZSCs) and $ZnSnO_3$ nanosheets (ZSSs) as anode material by two wet chemical routes [11]. ZSCs were prepared by dual-hydrolysis-assisted solution method, but ZSSs were prepared by hydrothermal route.

As clarified in figure 3a, the XRD patterns of the ZSCs and ZSSs powders and the diffraction profile revealed the phase purity of ZSCs and ZSSs nanosheets powder. SEM images showed that the edge size of the ZSCs sample is 50–100 nm while the ZSSs had rough surfaces with thicknesses ranging from 25–35 nm, as shown in figure 3b. These morphologies provided a short length for the lithium ions to diffuse, improving electrochemical performance. The proposed lithium insertion mechanism of ZSCs and ZSSs electrode material according to cyclic voltammetry is mentioned below [11]:

$$4\,Li^+ + ZnSnO_3 + 4\,e^- \longrightarrow Sn + 2\,Li_2O + ZnO \quad \text{..... (1)}$$

$$6\,Li^+ + ZnSnO_3 + 6\,e^- \longrightarrow Zn + Sn + 3\,Li_2O \quad \text{..... (2)}$$

$$x\,Li^+ + Sn + x\,e \longleftrightarrow 4\,Li_xSn, \qquad x \leq 4.4 \quad \text{..... (3)}$$

$$y\,Li^+ + Zn + y\,e \longleftrightarrow 4\,Li_yZn, \qquad y \leq 1 \quad \text{..... (4)}$$

According to equations (1) and (2), the lithiation process with $ZnSnO_3$ and alloy formation causes the reduction peaks at 0.69 and 0.05 V, respectively. The peaks 1.3 and 1.5 V are brought on by the oxidation of Sn and Zn, and peak 0.68 is induced by the dealloying process.

There is relevance between the size of particles and the quantity of lithium inserted (x). Submicrometer-sized particles could conduct only 0.03 mol of Li compared to 1 mol of Li for nanometer-sized particles. As a result, the ZSSs showed greater electrochemical performance than the ZSCs when their capacity for lithium storage was assessed.

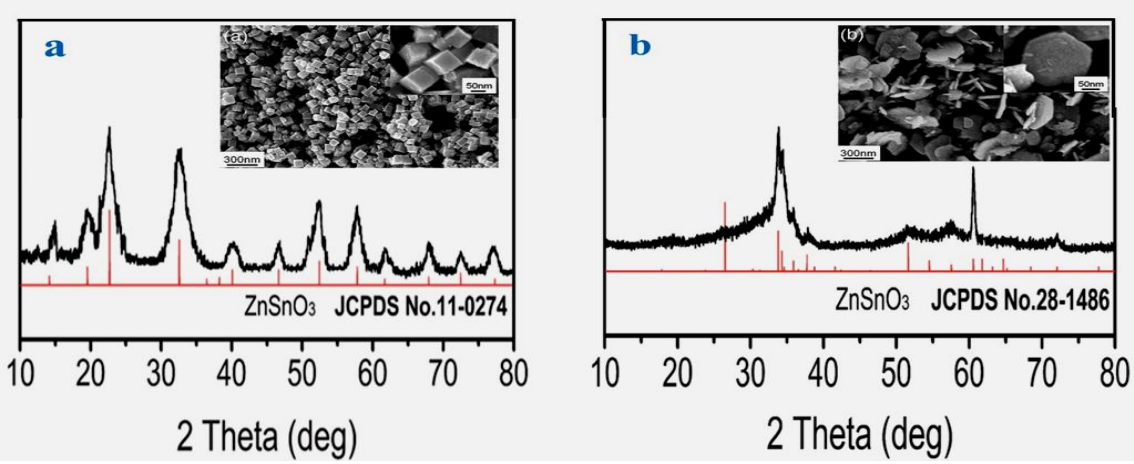

Fig. 3: XRD patterns and SEM images of a) ZSCs and b) ZSSs. Figure reprinted with permission from Royal Society of Chemistry (Ref. [11]).

The discharge/charge capacities of the 1st cycle of the ZSSs were 1390/1010 mAh g^{-1} with a 72.7% coulombic efficiency. ZSSs electrode provided a capacity twice as great as the ZSCs electrode after 50 cycles.

The hydrothermal treatment of the as-prepared powder produces relatively stable structures and low surface energies, which allow the electrode to release stress generated by the rapid volume expansion. On the other hand, amorphous $ZnSnO_3$ powders were prepared by Duan et al. using an alkaline etching technique. [12]. $ZnSnO_3$ with hollow nanoboxes microstructure showed better lithiation and delithiation processes than solid nanocubes electrodes, and the electrode displayed a discharge capacity of 80 mAh g^{-1} at a current density of 2.0 A g^{-1}. This result could be related to the lithium's ability to intercalate and deintercalate into the crystal without significant volume changes. Moreover, a simple chemical solution approach was used to synthesize amorphous hollow microcubes $ZnSnO_3$ powders with double-shell (D-ZSO) and yolk-shell (Y-ZSO). [13]. The D-ZSO electrode offered a first discharge/charge capacity of 2134/1204 mAh g^{-1} at a current density of 100 mA g^{-1}, equivalent to 56% coulombic efficiency. D-ZSO and Y-ZSO produced capacities of 426 and 224 mAh g^{-1}, respectively, at 1 A g^{-1}, demonstrating that D-ZSO has a superior rate performance than the Y-ZSO. Notably, compared to various $ZnSnO_3$ electrode materials previously described, the amorphous D-ZSO exhibited a significantly improved cycling stability. Researchers have used different techniques to overcome several cycling-related issues that ZSO faces, particularly significant pulverization and agglomeration during cycling, which results in capacity decay similar to that of most metal oxide anode materials. Combining with carbonaceous materials is considered the most successful technique, as carbon materials construct a conductive network to maintain volume change and promote the lithium ions' mobility into the $ZnSnO_3$ electrode, where the electrochemical stability was potentially improved. Table 1 summarizes the different types of carbonaceous materials composites with $ZnSnO_3$ anode materials.

Recent studies have focused on another type of perovskite material called nickel titanate ($NiTiO_3$). This material possessed distinctive properties, for example, good electronic transport, low cost, good ionic conductivity, and narrow band gap (~2.18 eV), which

enable it to be applied in several applications, such as the dielectric material, electrocatalysis, photocatalysis, supercapacitor, and metal-ion batteries [14-17]. $NiTiO_3$ has ilmenite crystal structures, at which the occupation of the octahedral sites (A) is by both Ni(II) and Ti(IV) ions [18]. $NiTiO_3$ was studied as a negative electrode material for LIB. It possesses a good theoretical capacity of 500 mAh g^{-1} with high rate capability. D. Das *et al.* synthesized polyhedral $NiTiO_3$ particles with 100–250 nm sizes by conventional sol-gel method. As can be seen in figure. 4, the $NiTiO_3$ CV curves were recorded at a sweep rate of 0.1 mV s^{-1} in a specified voltage range from 0.005-3 V (vs. Li/Li^+). [18]. There are two distinctive reduction peaks: one at 1.2 V was associated with the Ti^{4+} was reduced to Ti^{3+}, and the other at 0.28 V was attributed to Ni^{2+} was reduced to Ni (Eq.5). On the other hand, there are two oxidation peaks at around 1.6 V and 2.2 V (Eq. 6), respectively, which are induced by the oxidation of Ni/Ti and the decomposition of Li_2O as follows [18, 19]:

$$NiTiO_3 + 3\,Li^+ + 3\,e^- \rightarrow LiTiO_2 + Ni + Li_2O \quad \text{..... (5)}$$

$$Ni + Li_2O + LiTiO_2 \rightarrow 2\,Li + NiO + Li_{1-x}TiO_2 \quad (x \leq 0.5) \text{ ..... (6)}$$

At 50 mA g^{-1}, polyhedral $NiTiO_3$ can provide a capacity of 281 mA h g^{-1} after a hundred cycles. $NiTiO_3$ electrode offered a capacity of 130 mAh g^{-1} even after increasing the current density to 1.6 A g^{-1}. Lu et al. utilized microwave-assisted solvothermal to synthesize micro-rods $NiTiO_3$. At 0.1 C, the micro-rod $NiTiO_3$ electrode has a primary discharge/charge capacity of 750/460 mAh g^{-1}. [20]. The primary coulombic efficiency is relatively low, 61%, and increased after a few cycles to 90% during the cycling.

Table (1): Summarizes the different types of carbonaceous materials composites with $ZnSnO_3$ anode materials.

Anode material composite	Preparation Method	Capacity retention (mAh g^{-1})	Cycles (n)	I_d (mA g^{-1})	Ref
$ZnSnO_3$@C	Coprecipitation	817	100	100	[21]
$ZnSnO_3$@rGO aerogels	A Colloid Electrostatic Self-Assembly	745	100	100	[22]
$ZnSnO_3$@C	Hydrothermal Process	1107	200	100	[23]
$ZnSnO_3$@C	Coprecipitation	1060	100	200	[24]
$ZnSnO_3$@C/rGO	Coprecipitation + Colloid Electrostatic Self-Assembly	1040	45	100	[25]
$ZnSnO_3$@C	Facile Self-Templating	703	50	100	[26]
$ZnSnO_3$/rGO	Coprecipitation + Colloid Electrostatic Self-Assembly + Hydrothermal	718	100	100	[27]
$ZnSnO_3$/C	Hydrothermal	695	200	100	[28]
Ag-modified $ZnSnO_3$	Thermal Decomposition	464	45	300	[29]

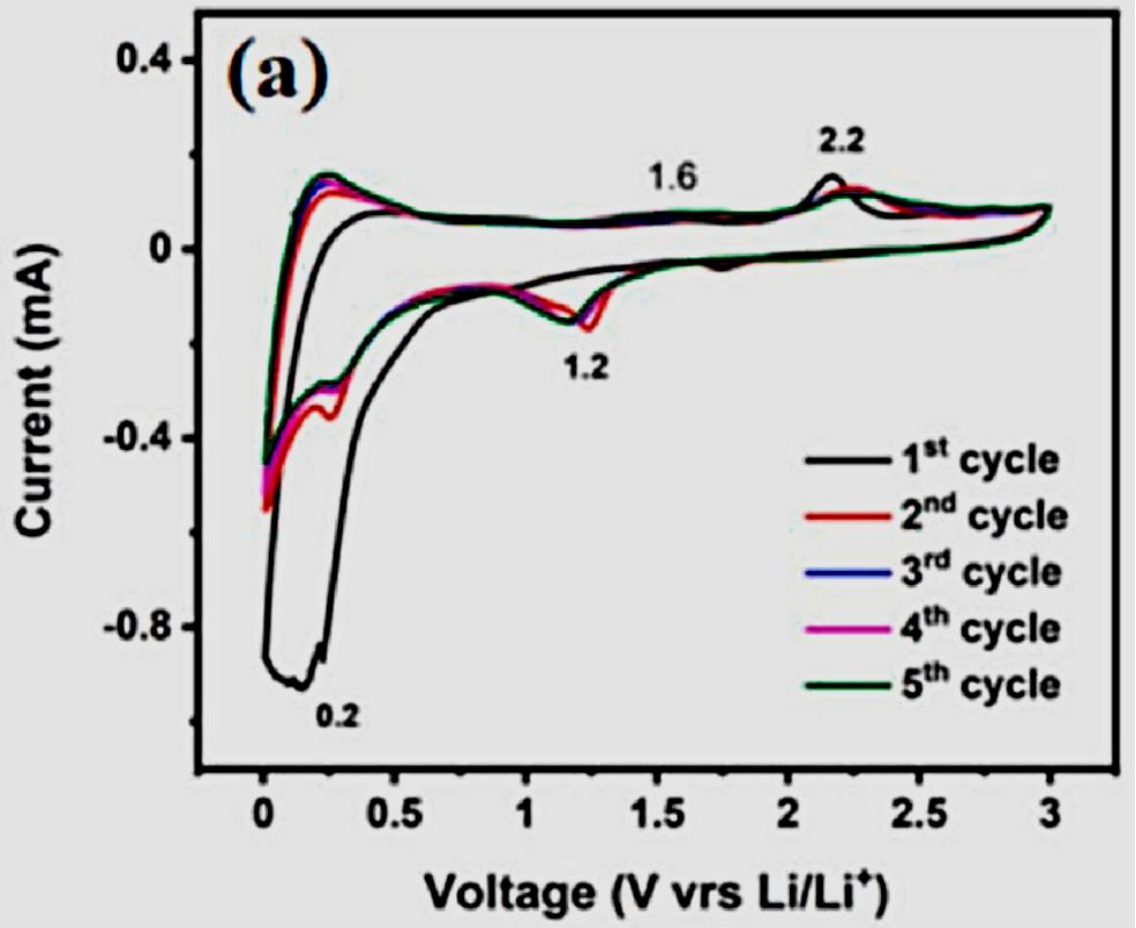

Fig. 4: CV curves of $NiTiO_3$ measured at 0.005-3 V (vs. Li/Li^+) at a sweep rate of 0.1 mV s^{-1}. Figure reprinted with permission from Elsevier (Ref. [18]).

Ilmenite $NiTiO_3$ structures with a size range of 0.8-1.2 µm were produced utilizing a quick one-pot method that relied on a glycerol/ethyl alcohol-mediated route [30]. The 3D flower-like electrode, which served as the anode for LIBs, showed reasonable electrochemical features toward Li^+ ions intercalation/deintercalation. According to investigations on cycle stability, the electrode may preserve its 400 mAh g^{-1} capacity afterwards 120 cycles at 100 mA g^{-1}.

A large surface area, which facilitates the transport of lithium ions, may be responsible for this. As shown in figure 5a, the capacity faded until the 40th cycle, gradually increasing, forming an "ascending-then-stable" pattern. This result might be attributed to the oxide activation, and kinetically driven electrolyte decomposition may create a polymeric gel-like layer, improving capacity.

$NiTiO_3$ rate capability by varied current densities from 0.1 to 1 A g^{-1} was investigated and depicted in figure 5b. At 0.1 A g^{-1}, the flower-like $NiTiO_3$ has a capacity of 475 mAh g^{-1}.

The electrode remains to provide capacities of 356, 276, and 235 mAh g^{-1} when the current density increases to 0.2, 0.5, and 1 A g^{-1}, respectively. The flower-like $NiTiO_3$

exhibited a virtual performance rate of a capacity of ~390 mAh g^{-1} after 80 cycles, at which the current density gradually recovered to its initial value of 0.1 A g^{-1}.

This performance may be attributed to the features of flower-like $NiTiO_3$, which adopts a 3D network in the crystal structure that acts as a diffusion region for Li^+ ions. To elevate the electrochemical performance of $NiTiO_3$ [30]. F. Huang *et al.* proposed using a simple plasma-enhanced chemical vapor deposition to encapsulate $NiTiO_3$ nanorods inside a few graphene layers [31].

After 500 cycles at the 0.2 mA g^{-1} current density, the capacity of $NiTiO_3$@graphene anode was 556 mAh $g^{-1,}$ besides 83% capacity retention. NiTiO3@graphene electrodes are differentiated by their superior rate performances, in which they can deliver capacities of 414 and 376 mAh g^{-1} at 2 and 5 A g^{-1}, separately, as high cycling currents. The excellent electrochemical performances of $NiTiO_3$@graphene electrodes were attributed to the graphene coating improving the electrical connectivity during cycling.

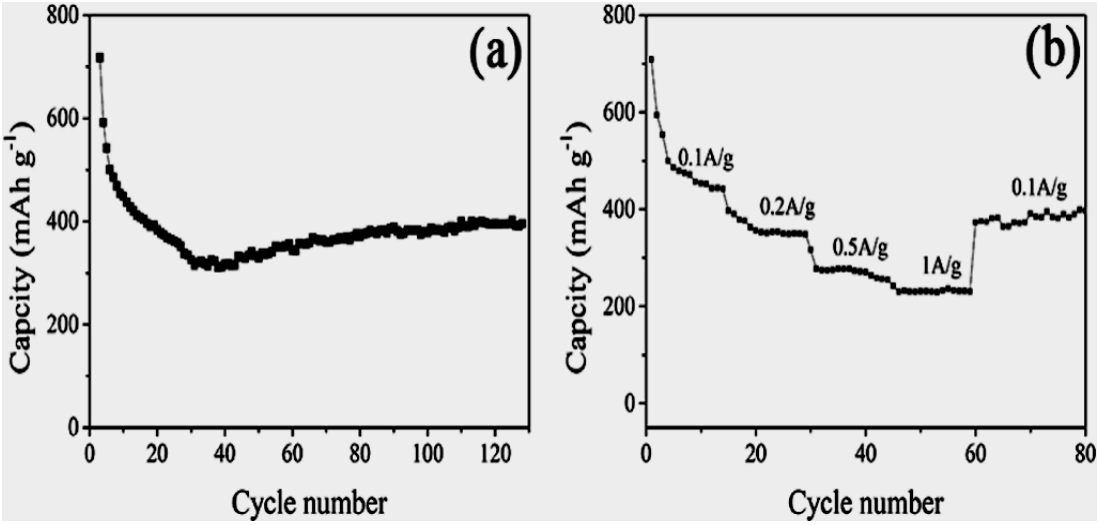

Fig. 5: (a) Cycling performance at a current density of 0.1 A g^{-1}, (b) The rate capability at various current densities. Figure reprinted with permission from Elsevier (Ref. [30]).

$CaSnO_3$ has also been evaluated as a potential anode material for LIBs. The lithiation/delithiation mechanism is similar to $ZnSnO_3$ and was declared as follows:

$$CaSnO_3 + 4\ Li^+ + 4\ e^- \longrightarrow CaO + 2\ Li_2O + Sn \quad \text{..... (7)}$$

$$4.4\ Li^+ + 4.4\ e^- + Sn \longleftrightarrow Li_{4.4}Sn \quad \text{..... (8)}$$

Due to the strong bonding between Ca and O, ZnO and CaO cannot be reduced by Li^+ to the Ca-metal. Porous flower-like $CaSnO_3$ powder was prepared via the hydrothermal method. After 50 cycles at 60 mA g^{-1}, the $CaSnO_3$ anode capacity was 547 mAh g^{-1} [32]. Using a sol-gel method, N. Sharma et al. synthesized $CaSnO_3$ with particle sizes ranging from 200 to 300 nm at high temperatures.

After 45 cycles at 60 mA g^{-1}, the $CaSnO_3$ anode offered a 380 mAh g^{-1} discharge capacity [33]. To further improve the electrochemical accomplishment of $CaSnO_3$, X. Hu et al. developed a composite in which a $CaSnO_3$ nanotube was prepared and then coated with carbon to create a core-shell composite [34]. The core-shell composite electrode could provide a 150 mAh g^{-1} capacity at a 60 mA g^{-1} current density after 30 cycles.

The electrochemical behavior of various cathode materials has also been enhanced by surface coating with perovskite materials in LIBs. $LiNi_{0.5}Mn_{1.5}O_4$ (LNMO) with a spinel crystal structure [35, 36] is considered a high-voltage cathode material. With the Ni^{2+} ions and the Mn^{4+} ions, it is an interesting derivative of $LiMn_2O_4$ with a reasonable capacity and high cycle stability. The exchange of 0.5 Li^+ per metal occurred for the Ni^{2+} ion but not for the Mn ion, which decreased the dissolution of Mn. However, the high-voltage LNMO is reactive toward electrolytes, leading to side reactions with capacity fading.

Surface modification was caused by $Li_{0.33}La_{0.56}TiO_3$ (LLTO) coating on the surface of LNMO and was reported by S. Luo *et al.* Perovskite LLTO has an excellent ionic conductivity of 10-3 S cm^{-1}, which increases the rate at which Li^+ ions move through the composite [36]. LNMO@LLTO composites were produced by the sol-gel method. They investigated the impact of LLTO amounts of 1, 3, and 5% of the material's total weight on the electrochemical performance of the LNMO. LLTO (3% wt.) was found to have a high energy density and excellent rate capability [35, 36].

P. Guan *et al.* also explored the influence of the surface coating by the $SrTiO_3$ (STO) perovskite powder on $LiNi_{0.8}Co_{0.1}Mn_{0.1}O_2$ (NCM811) cycling stability and rate capability [37]. The STO nanoparticles were initially synthesized using a solvothermal procedure and were added in amounts of 1, 3, and 5 wt.% to NCM811 via the wet chemical method. The NCM811 modified with STO indicated reduced initial discharge capacity due to STO being electrochemically inactive.

Galvanostatic charge-discharge curves were used to investigate the electrochemical characteristics of STO-NCM811, as illustrated in figure 6. The first cycle charge/discharge capacities of 253/214, 235/213, 224/207, and 215/198 mAh g^{-1} at 0.1C were exhibited by introducing STO-811 at 1, 2, and 3 wt.%, respectively. Figure 6b demonstrates that the discharge capacity retentions of the 1, 3, and 5% STO- NCM811 are 71.5, 89.8, and 83.2%, respectively.

These retentions are considerably higher than the NCM811 (65.3%) at 1C after 200 cycles. The rate capability of STO-NCM811 at different C-rates, from the lowest 0.1 to the highest 10 C, was studied as presented in figure 6c. Interestingly, among all investigated cells, 3% STO-811 had the best rate performance; specifically, at 10 C rate, this sample kept 141.3 mAh g^{-1} on average, whereas others retained less than 130 mAh g^{-1}. After the current density gradually returned to 0.1 C, the 3 % STO-811 exhibited a high rate capability with a capacity of 200 mAh g^{-1}, which was higher than that of 165 mAh g^{-1} for the NCM811 after 40 cycles.

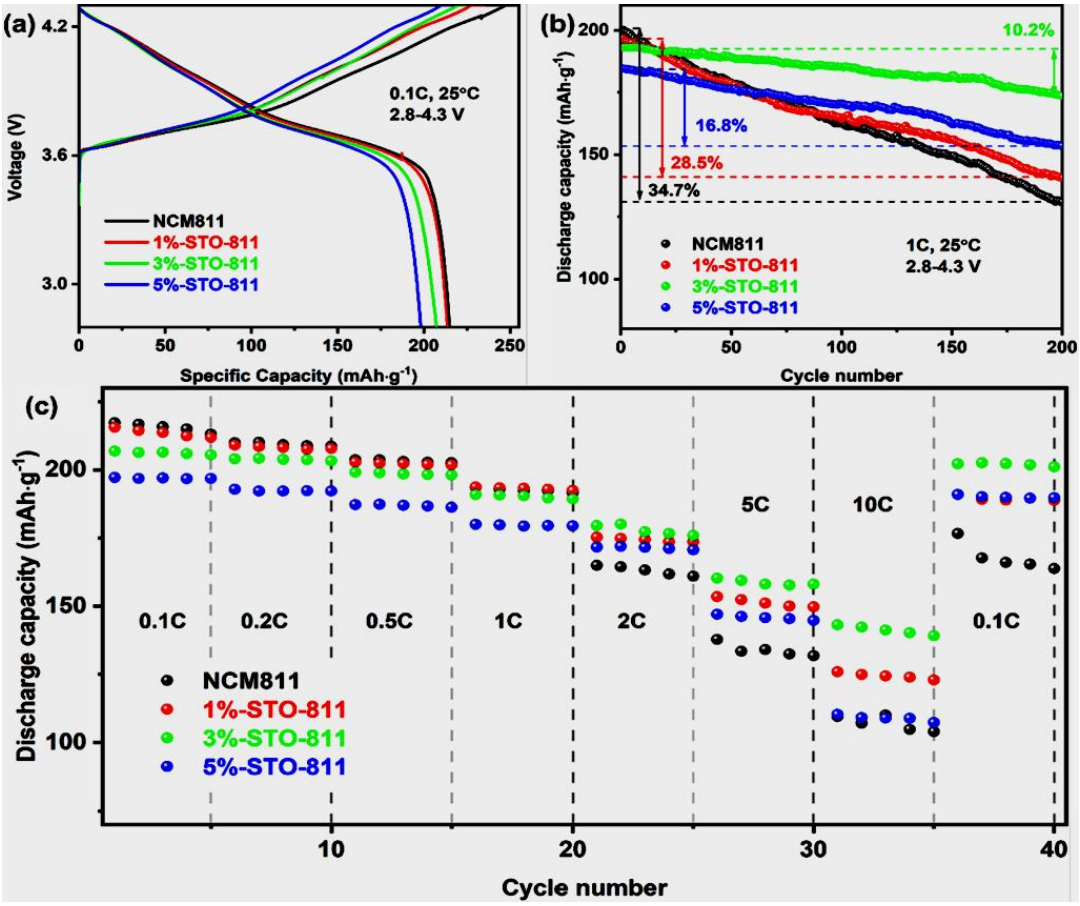

Fig. 6: (a) Initial charge-discharge profile, (b) Cycling stability of uncoated and coated NCM811 after 200 cycles, (c) rate capability at different C-rates. Figure reprinted with permission from Elsevier (Ref. [37]).

3. SODIUM-ION BATTERY (SIB)

Due to Na and Li having similar physical and chemical characteristics, SIBs and LIBs are quite identical. The most promising prospects for extensive energy storage are SIBs owing to their minimal expense, naturally abundant Na, besides low toxicity. However, the high ionic radius of Na^+ (1.02 Å) in SIBs frequently leads to many phases and substantial structural changes, which invariably induce mechanical integrity damage and capacity fading. Researchers studied various electrode materials with different storage mechanisms. Hard carbon is an intercalation electrode material that stores Na^+ ions via a solid-solution reaction. It has a large capacity and good cycling behavior, but its low intercalated potential of < 0.1V leads to dendrite formation. Furthermore, the insertion of Na in conversion-based (Fe_3O_4, FeS, and MoS_2) and alloying/dealloying electrode materials (Sb, P, and Sn) lead to volume expansion and pulverization of electrode material with gradual capacity fading. Therefore, developing new electrode materials with excellent electrochemical performance is important [38-41].

$Ce_{1/3}NbO_3$ (CNO) is considered an intercalation perovskite anode material. Because of the proper cation vacancies and the storage of Na^+'s charge in the interfacial region on the surface of CNO particles, CNO had an exceptional Na^+ storage capacity of 141.3 mAh g^{-1}. R. Che *et al.* prepared CNO-fibers by electrospinning. One electron transfer

during intercalation/ deintercalation was attributed to redox couples of Nb^{5+}/Nb^{4+}. It was revealed from CV curves in which a pair of reduction/oxidation peaks at ≈0.46/≈0.41 V originated redox couples of Nb^{5+}/Nb^{4+}. CNO-fibers revealed a capacity of 141.3 mAh g^{-1} at 0.1 C [42].

CNO further demonstrated outstanding endurance when cycling, retaining 90.2% of its capacity after a thousand cycles at 1 C, 99.4% after 2k cycles at 5 C, and 96.5% after 10k cycles at 10 C. The cycling's outstanding achievement was ascribed to the "zero-stain" sodium ions storing function, with the largest volume variation of the unit cell caused by Na^+ insertion/extraction calculated as being 0.38%. CNO is a potential replacement for SIBs since it has a long life.

$Na_{0.5}Bi_{0.5}TiO_3$ (NBTO) [43] is another potential anode material for SIBs. Through using the conversion redox process, NBTO could react with Na. A pair of cathodic peaks at 0.62 V and 0.35 V were identified based on CV curves caused by adding Na to NBTO. On the other hand, as seen in figure 7, the two anodic peaks at 0.69 V and 0.8 V were attributable to the Na being ejected from NBTO. After 50 cycles, the perovskite $Na_{0.5}Bi_{0.5}TiO_3$ can deliver a capacity of 215 mAh g^{-1} at the current density of 0.1 A g^{-1}.

$NiTiO_3$ was proven as a promising negative electrode for SIBs [44]. Powders of $NiTiO_3$ were prepared by the conventional sol-gel technique, which was then immediately uploaded with a $NiTiO_3$-GO composite. The CV profiles determined that the decrease of Ti^{4+} and Ni^{2+} resulted in two cathodic peaks at 1.4 and 0.4 V. Meanwhile, 0.1 V and 2.1 V anodic peaks were ascribed to material desodiation and Ni and Ti oxidation. With a current density of 0.1 A g^{-1}, the $NiTiO_3$-GO composite had an initial capacity of 800 mAh g^{-1}, with capacity retention of 290 mAh g^{-1} after 100 cycles.

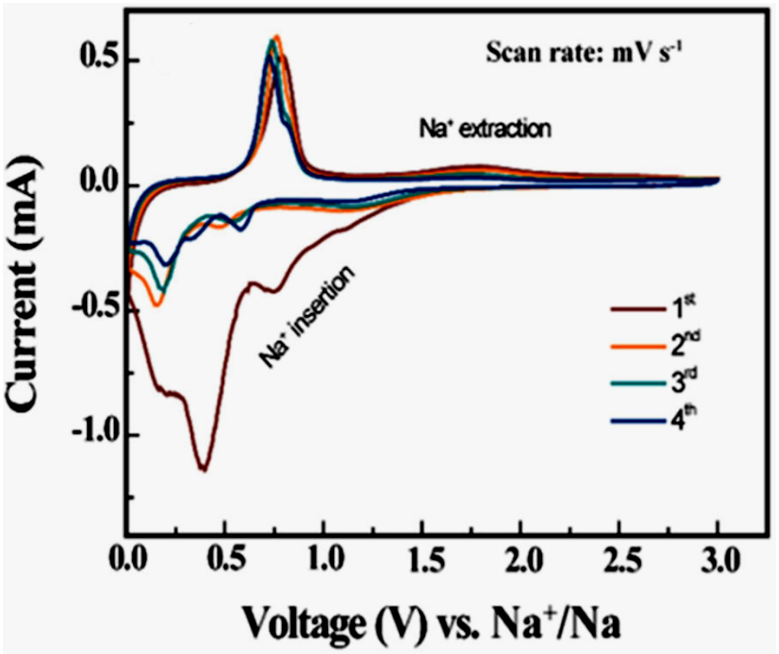

Fig. 7: CV curves of NBTO anode versus Na/Na^+ at a sweep rate of 0.1 mV s^{-1}. Figure reprinted with permission from Springer Nature (Ref. [43]).

Hybrid perovskites are currently attractive in many applications, such as solar cells, sensors, energy storage devices, light-emitting devices, and photocatalytic hydrogen generation. The chemical composition of hybrid perovskites with ABX_3, where A = $CH_3NH^+_3$, $CH(NH_2)^{2+}$; and B is a metal = Pb^{2+}, Sn^{2+}, X = Br^-, I^-, Cl^- is called organic-inorganic perovskites.

The lithiation mechanism of organic-inorganic perovskite compounds has been extensively studied. Topological insertion occurred as lithium ions started to enter the perovskite with a deformed structure. Afterwards, alloying procedures were performed, adding more and more lithium ions to the perovskite [45].

Several LiPb phases, such as $Li_{3.5}Pb$, Li_3Pb, Li_8Pb_3, and LiPb, have been detected in the same voltage range for electrodes made of pure lead metal as a result of the LiPb alloying that began during the lithiation process at x > 2. Thus, the number of alloyed Li ions can reach a molar content of up to x = 3. H. Kong *et al.* prepared 1D perovskite $C_4H_{20}N_4PbBr_6$ by a simple wet chemical method [46].

Figure 8a illustrates the CV curves for the $C_4H_{20}N_4PbBr_6$ electrode across the voltage range of 0 V to 2.0 V at a scan rate of 0.1 mV s^{-1}. The formation of the solid electrolyte interphase (SEI) was responsible for the cathodic peak at 0.7 V [47].

The multi-step process for the formation of the lithium-lead alloy was indicated by the two peaks at around 0.5 V and 0.2 V. The oxidation peaks at 1.7, 0.7, and 0.5 V were attributed to the dealloying reactions of LiPb, Li_3Pb, and $Li_{3.2}Pb$.

According to figure 8b, a 1D perovskite $C_4H_{20}N_4PbBr_6$ battery with a current density of 0.15 A g^{-1} produced a 1632.8 mAh g^{-1} initial specific capacity and 598.0 mAh g^{-1} capacity retention after 50 cycles.

The 1D perovskite $C_4H_{20}N_4PbBr_6$ demonstrated greater cycling stability (figure 8c), with the electrode keeping its 449.9 mAh g^{-1} specific capacity even after 500 cycles. [46].

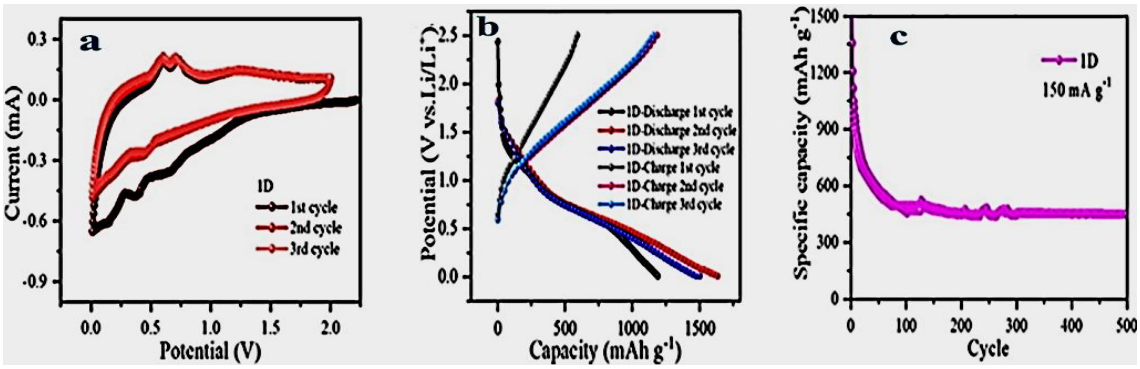

Fig. 8: 1D perovskite $C_4H_{20}N_4PbBr_6$. (a) Cyclic voltammetry measurements, b) charge-discharge pattern, c) Cycling stability at 0.15 A g^{-1}. Figure reprinted with permission from Elsevier (Ref. [46]).

The electrochemical properties of different types of organic-inorganic perovskites are listed in table 2.

Table (2): Summarizes the various types of organic-inorganic perovskite anode materials for LIBs.

Anode material	Preparation Method	Capacity retention (mAh g^{-1})	Cycles (n)	Current density (mA g^{-1})	Ref
$CH_3NH_3PbBr_3$	Hydrothermal Process	121	200	200	[48]
$CH_3NH_3PbI_3$	Hydrothermal Process	9	100	200	[48]
$CH_3NH_3PbBr_3$	Wet chemical Process	100	30	50	[49]
1D $C_6H_9I_3NOPb$	Wet chemical Process	585	50	100	[50]
2D $C_4H_9NH_3)_2PbI_4$	Wet chemical Process	213	50	100	[50]
3D $CH_3NH_3PbI_3$	Wet chemical Process	213	50	100	[50]
$CH_3NH_3NiCl_3$	Wet chemical Process	350	19	32	[51]

4. Conclusions and Future Research Outlook

The advantages of perovskites used in MIBs are high theoretical capacity, safety concerns, widespread availability, and low processing cost. However, perovskites suffer from volume expansion during the lithiation and de-lithiation process, which causes accelerated capacity diminishing and poor rate capability. We have mentioned some effective strategies, such as designing different micro-nano-morphologies (microcubic, plates, nanoboxes, fibers, nanorods, nanoparticles). Also, perovskites with various carbonaceous materials formed composites effectively enhanced electrical conductivity and mechanical strength. The produced carbon-based composites had a large specific surface area, a porous structure, and rapid electron transport kinetics since they efficiently reduced the stress and volume variations. The research on perovskite-based materials will undoubtedly continue, and many new applications based on all these materials will be pictured shortly.

5. References

[1] Johnsson, M. and Lemmens, P. (2007): "Crystallography and chemistry of Perovskites, in Handbook of Magnetism and Advanced Magnetic Materials".

[2] Fayed, M. G.; Attia, S. Y.; Barakat, Y. F.; El-Shereafy, E.; Rashad, M. and Mohamed, S. G. (2021): "Carbon and nitrogen co-doped MoS_2 nanoflakes as an electrode material for lithium-ion batteries and supercapacitors". Sustainable Materials and Technologies. **29**: p. e00306.

[3] Manthiram, A. (2017): "An outlook on lithium-ion battery technology". ACS central science. **3**(10): p. 1063-1069.

[4] Wu, J.; Cao, Y.; Zhao, H.; Mao, J. and Guo, Z. (2019): "The critical role of carbon in marrying silicon and graphite anodes for high-energy lithium-ion batteries". Carbon Energy. **1**(1): p. 57-76.

[5] Zhang, H.; Yang, Y.; Ren, D.; Wang, L. and He, X. (2021): "Graphite as anode materials: Fundamental mechanism, recent progress and advances". Energy Storage Materials. **36**: p. 147-170.

[6] Ahmed, S.; Bloom, I.; Jansen, A. N.; Tanim, T.; Dufek, E. J.; Pesaran, A.; Burnham, A.; Carlson, R. B.; Dias, F. and Hardy, K. (2017): "Enabling fast charging–A battery technology gap assessment". J. Power Sources. **367**: p. 250-262.

[7] Jung, H.-G.; Jang, M. W.; Hassoun, J.; Sun, Y.-K. and Scrosati, B. (2011): "A high-rate long-life $Li_4Ti_5O_{12}$/Li [NiO. 45CoO. 1Mn1. 45] O_4 lithium-ion battery". Nature communications. **2**(1): p. 1-5.

[8] Seo, J.-H.; Verlinde, K.; Rajagopalan, R.; Gomez, E. D.; Mallouk, T. E. and Randall, C. A. (2019): "Cold sintering process for fabrication of a high volumetric capacity $Li_4Ti_5O_{12}$ anode". Materials Science and Engineering: B. **250**: p. 114435.

[9] Rovisco, A.; Branquinho, R.; Martins, J.; Fortunato, E.; Martins, R. and Barquinha, P. (2019): "Growth mechanism of seed-layer free $ZnSnO_3$ nanowires: effect of physical parameters". Nanomaterials. **9**(7): p. 1002.

[10] Song, P.; Wang, Q. and Yang, Z. (2011): "Biomorphic synthesis of $ZnSnO_3$ hollow fibers for gas sensing application". Sensors and Actuators B: Chemical. **156**(2): p. 983-989.

[11] Chen, Y.; Qu, B.; Mei, L.; Lei, D.; Chen, L.; Li, Q. and Wang, T. (2012): "Synthesis of $ZnSnO_3$ mesocrystals from regular cube-like to sheet-like structures and their comparative electrochemical properties in Li-ion batteries". J. Mater. Chem. **22**(48): p. 25373-25379.

[12] Duan, J.-F.; Hou, S.-C.; Chen, S.-G. and Duan, H.-G. (2014): "Synthesis of amorphous $ZnSnO_3$ hollow nanoboxes and their lithium storage properties". Mater. Lett. **122**: p. 261-264.

[13] Ma, Y.; Xie, Q.; Liu, X.; Zhao, Y.; Zeng, D.; Wang, L.; Zheng, Y. and Peng, D.-L. (2015): "Synthesis of amorphous $ZnSnO_3$ double-shell hollow microcubes as advanced anode materials for lithium ion batteries". Electrochim. Acta. **182**: p. 327-333.

[14] Regulska, E.; Breczko, J. and Basa, A. (2022): "Multifunctional $NiTiO_3$-decorated-rGO nanostructure for energy storage, electro-and photocatalytic applications". Diamond Relat. Mater. **128**: p. 109310.

[15] Viet, C. D.; Nga, N. T.; Ngoc, T. V. D.; Van Dung, N. and Bac, L. H. (2022): "Structural, electrical and ferroelectric properties of $NiTiO_3$ synthesized by citrate-gel method". Vietnam Journal of Science and Technology. **60**(2): p. 245-256.

[16] Thiagarajan, V.; Karthikeyan, P.; Manoharan, R.; Sampath, S.; Hernández-Ramírez, A.; Sánchez-Castro, M.; Alonso-Lemus, I. and Rodríguez-Varela, F. (2018): "Pt-Ru-$NiTiO_3$ nanoparticles dispersed on vulcan as high performance electrocatalysts for the methanol oxidation reaction (MOR)". Electrocatalysis. **9**(5): p. 582-592.

[17] Wang, L.; Yang, G.; Wang, S.; Wang, J.; Nasir, M. S.; Wang, C.; Peng, S.; Yan, W. and Ramakrishna, S. (2019): "Fabrication of hierarchically one-dimensional ZnxCd1-xS/$NiTiO_3$ nanostructures and their enhanced photocatalytic water splitting activity". Int. J. Hydrogen Energy. **44**(59): p. 30974-30985.

[18] Majumder, T.; Das, D. and Majumder, S. B. (2021): "Investigations on the electrochemical characteristics of electrophoretically deposited $NiTiO_3$ negative electrode for lithium-ion rechargeable cells". J. Phys. Chem. Solids. **158**: p. 110239.

[19] Huang, Z.-D.; Zhang, T.-T.; Lu, H.; Masese, T.; Yamamoto, K.; Liu, R.-Q.; Lin, X.-J.; Feng, X.-M.; Liu, X.-M. and Wang, D. (2018): "Grain-boundary-rich mesoporous $NiTiO_3$ micro-prism as high tap-density, super rate and long life anode for sodium and lithium ion batteries". Energy Storage Materials. **13**: p. 329-339.

[20] Lu, C.-H.; Naresh, N.; Kumar, P. S. and Som, S. (2019): "Microwave-assisted solvothermal synthesis and electrochemical characterizations of ternary perovskite $NiTiO_3$ anode materials for lithium-ion batteries". Ceram. Int. **45**(15): p. 19517-19521.

[21] Ma, J.; Zhang, Z.; Mentbayeva, A.; Yuan, G.; Wang, B.; Wang, H. and Wang, G. (2019): "Enhanced electrochemical performance of hollow heterostructured carbon encapsulated znic metastanate microcube composite for lithium-ion and sodium-ion batteries". Electrochim. Acta. **312**: p. 31-44.

[22] Wang, Y.; Li, D.; Liu, Y. and Zhang, J. (2016): "Self-assembled 3D $ZnSnO_3$ hollow cubes@ reduced graphene oxide aerogels as high capacity anode materials for lithium-ion batteries". Electrochim. Acta. **203**: p. 84-90.

[23] Luo, P.; Zhang, H.; Liu, L.; Fang, L. and Wang, Y. (2016): "Sandwich-like nanostructure of amorphous $ZnSnO_3$ encapsulated in carbon nanosheets for enhanced lithium storage". Electrochim. Acta. **219**: p. 734-741.

[24] Han, F.; Li, W. C.; Lei, C.; He, B.; Oshida, K. and Lu, A. H. (2014): "Selective formation of carbon-coated, metastable amorphous $ZnSnO_3$ nanocubes containing mesopores for use as high-capacity lithium-ion battery". Small. **10**(13): p. 2637-2644.

[25] Jiang, R.; Wang, Y.; Gao, C.; Li, A.; Liu, Y.; Li, D. and Zhang, J. (2017): "Hollow $ZnSnO_3$ cubes@ carbon/reduced graphene oxide ternary composite as anode of lithium ion batteries with enhanced electrochemical performance". Ceram. Int. **43**(15): p. 11556-11562.

[26] Xie, Q.; Ma, Y.; Zhang, X.; Guo, H.; Lu, A.; Wang, L.; Yue, G. and Peng, D.-L. (2014): "Synthesis of amorphous $ZnSnO_3$-C hollow microcubes as advanced anode materials for lithium ion batteries". Electrochim. Acta. **141**: p. 374-383.

[27] Ma, Y.; Jiang, R.; Li, D.; Dong, Y.; Liu, Y. and Zhang, J. (2018): "Embedding ultrafine $ZnSnO_3$ nanoparticles into reduced graphene oxide composites as high-performance electrodes for lithium ion batteries". Nanotechnology. **29**(19): p. 195401.

[28] Wang, K.; Zhang, S.; Hou, Z.; Wang, L.; An, P.; Jia, J.; Li, Y. and Zhang, P. (2022): "Nanofibrous $ZnSnO_3$/C composite derived from natural cellulose substance as an enhanced lithium-ion battery anode". Mater. Lett.: p. 133435.

[29] Chen, X.; Huang, Y.; Huang, H.; Wang, M. and Wang, K. (2015): "Silver-modified hollow $ZnSnO_3$ boxes as high capacity anode materials for Li-ion batteries". Mater. Lett. **149**: p. 33-36.

[30] Wang, Y.; Chen, X.; Wang, Q.; Zeng, Y.; Liao, K.; Zhang, S. and Zhong, Q. (2019): "Novel 3D hierarchical bifunctional $NiTiO_3$ nanoflower for superior visible light photoreduction performance of CO_2 to CH_4 and high lithium storage performance". Energy. **169**: p. 580-586.

[31] Xu, J.; Ding, W.; Zhao, W.; Zhao, W.; Hong, Z. and Huang, F. (2017): "In situ growth enabling ideal graphene encapsulation upon mesocrystalline $MTiO_3$ (M= Ni, Co, Fe) nanorods for stable lithium storage". ACS Energy Letters. **2**(3): p. 659-663.

[32] Zhao, S.; Bai, Y. and Zhang, W.-F. (2010): "Electrochemical performance of flower-like $CaSnO_3$ as high capacity anode material for lithium-ion batteries". Electrochim. Acta. **55**(12): p. 3891-3896.

[33] Sharma, N.; Shaju, K.; Rao, G. S. and Chowdari, B. (2002): "Sol–gel derived nano-crystalline $CaSnO_3$ as high capacity anode material for Li-ion batteries". Electrochem. Commun. **4**(12): p. 947-952.

[34] Hu, X.; Xiao, T.; Huang, W.; Tao, W.; Heng, B.; Chen, X. and Tang, Y. (2012): "Synthesis, characterization of core–shell carbon-coated $CaSnO_3$ nanotubes and their performance as anode of lithium ion battery". Appl. Surf. Sci. **258**(17): p. 6177-6183.
[35] Zhu, Y.-R.; Yi, T.-F.; Li, X.-Y.; Xie, Y. and Luo, S. (2019): "Improved rate performance of LiNi0. 5Mn1. $5O_4$ as cathode of lithium-ion battery by Li0. 33La0. $56TiO_3$ coating". Mater. Lett. **239**: p. 56-58.
[36] Bohnke, O. (2008): "The fast lithium-ion conducting oxides Li3xLa2/3− $xTiO_3$ from fundamentals to application". Solid State Ionics. **179**(1-6): p. 9-15.
[37] Guan, P.; Zhu, Y.; Li, M.; Zeng, T.; Li, X.; Tian, R.; Sharma, N.; Xu, Z.; Wan, T. and Hu, L. (2022): "Enhancing cyclic and in-air stability of Ni-Rich cathodes through perovskite oxide surface coating". J. Colloid Interface Sci. **628**: p. 407-418.
[38] Cho, J. S.; Park, J.-S. and Kang, Y. C. (2017): "Porous FeS nanofibers with numerous nanovoids obtained by Kirkendall diffusion effect for use as anode materials for sodium-ion batteries". Nano Research. **10**(3): p. 897-907.
[39] Kim, J.-H.; Kim, D. K.; Kim, J.-H. and Kim, D. K. (2018): "Conversion-alloying anode materials for na-ion batteries: recent progress, challenges, and perspective for the future". Journal of the Korean Ceramic Society. **55**(4): p. 307-324.
[40] David, L.; Bhandavat, R. and Singh, G. (2014): "MoS_2/graphene composite paper for sodium-ion battery electrodes". ACS nano. **8**(2): p. 1759-1770.
[41] Wei, G.; Zhou, Z.; Zhao, X.; Zhang, W. and An, C. (2018): "Ultrathin metal–organic framework nanosheet-derived ultrathin Co_3O_4 nanomeshes with robust oxygen-evolving performance and asymmetric supercapacitors". ACS applied materials & interfaces. **10**(28): p. 23721-23730.
[42] Liang, G.; Yang, L.; Xiong, X.; Pei, K.; Zhao, X.; Wang, C.; You, W.; Liu, X.; Zhang, X. and Che, R. (2022): "Interfacial space charge enhanced sodium storage in a zero-strain cerium niobite perovskite anode". Adv. Funct. Mater. **32**(43): p. 2206129.
[43] Bharathi, K. K.; Moorthy, B.; Dara, H. K.; Durai, L. and Kim, D. K. (2019): "Electrochemical properties of Na0. 5Bi0. $5TiO_3$ perovskite as an anode material for sodium ion batteries". Journal of Materials Science. **54**(20): p. 13236-13246.
[44] Majumder, T.; Das, D. and Majumder, S. B. (2021): "Nickel Titanate-GO composite as negative electrode for lithium and sodium ion batteries". Mater. Lett. **301**: p. 130293.
[45] Vicente, N.; Bresser, D.; Passerini, S. and Garcia-Belmonte, G. (2019): "Probing the 3-step lithium storage mechanism in $CH_3NH_3PbBr_3$ perovskite electrode by Operando-XRD analysis". ChemElectroChem. **6**(2): p. 456-460.
[46] Kong, H.; Wu, J.; Han, Y.; Zhang, Y.; Zhou, N.; Chen, Q.; Sun, W.; Zhou, H. and Peng, L.-M. (2022): "One-dimensional perovskite-based Li-ion battery anodes with high capacity and cycling stability". Journal of Energy Chemistry. **72**: p. 73-80.
[47] Haruyama, J.; Sodeyama, K.; Han, L. and Tateyama, Y. (2015): First-principles study of ion diffusion in perovskite solar cell sensitizers". J. Am. Chem. Soc. **137**(32): p. 10048-10051.
[48] Xia, H.-R.; Sun, W.-T. and Peng, L.-M. (2015): "Hydrothermal synthesis of organometal halide perovskites for Li-ion batteries". Chem. Commun. **51**(72): p. 13787-13790.

[49] Vicente, N. and Garcia-Belmonte, G. (2017): "Methylammonium lead bromide perovskite battery anodes reversibly host high Li-ion concentrations". The journal of physical chemistry letters. **8**(7): p. 1371-1374.

[50] Tathavadekar, M.; Krishnamurthy, S.; Banerjee, A.; Nagane, S.; Gawli, Y.; Suryawanshi, A.; Bhat, S.; Puthusseri, D.; Mohite, A. D. and Ogale, S. (2017): "Low-dimensional hybrid perovskites as high performance anodes for alkali-ion batteries". Journal of Materials Chemistry A. **5**(35): p. 18634-18642.

[51] López, L. T.; Ramírez, D.; Jaramillo, F. and Calderón, J. A. (2020): "Novel hybrid organic-inorganic $CH_3NH_3NiCl_3$ active material for high-capacity and sustainable lithium-ion batteries". Electrochim. Acta. **357**: p. 136882.